REGULAR ARTICLE

blood advances

Human *MYD88*^{L265P} is insufficient by itself to drive neoplastic transformation in mature mouse B cells

Tomasz Sewastianik,[1,2,*] Maria Luisa Guerrera,[1,3,*] Keith Adler,[1] Peter S. Dennis,[1] Kyle Wright,[4] Vignesh Shanmugam,[4] Ying Huang,[1] Helen Tanton,[1] Meng Jiang,[1] Amanda Kofides,[3] Maria G. Demos,[3] Audrey Dalgarno,[5] Neil A. Patel,[5] Anwesha Nag,[5] Geraldine S. Pinkus,[4] Guang Yang,[3] Zachary R. Hunter,[3] Petr Jarolim,[4] Nikhil C. Munshi,[6] Steven P. Treon,[3] and Ruben D. Carrasco[1,4]

[1]Department of Oncologic Pathology, Dana-Farber Cancer Institute, Harvard Medical School, Boston, MA; [2]Department of Experimental Hematology, Institute of Hematology and Transfusion Medicine, Warsaw, Poland; and [3]Bing Center for Waldenström's Macroglobulinemia, Dana-Farber Cancer Institute, [4]Department of Pathology, Brigham & Women's Hospital, [5]Center for Cancer Genome Discovery, Dana-Farber Cancer Institute, and [6]Jerome Lipper Myeloma Center, Dana-Farber Cancer Institute, Harvard Medical School, Boston, MA

Key Points

- *MYD88*^{L265P} mutation is insufficient to drive malignant transformation by itself.
- *MYD88*^{L265P} promotes a non-clonal B-cell lymphoproliferative disorder with some features of LPL/WM and the potential to transform to DLBCL in older mice.

MYD88^{L265P} is the most common mutation in lymphoplasmacytic lymphoma/Waldenström macroglobulinemia (LPL/WM) and one of the most frequent in poor-prognosis subtypes of diffuse large B-cell lymphoma (DLBCL). Although inhibition of the mutated MYD88 pathway has an adverse impact on LPL/WM and DLBCL cell survival, its role in lymphoma initiation remains to be clarified. We show that in mice, human *MYD88*^{L265P} promotes development of a non-clonal, low-grade B-cell lymphoproliferative disorder with several clinicopathologic features that resemble human LPL/WM, including expansion of lymphoplasmacytoid cells, increased serum immunoglobulin M (IgM) concentration, rouleaux formation, increased number of mast cells in the bone marrow, and proinflammatory signaling that progresses sporadically to clonal, high-grade DLBCL. Murine findings regarding differences in the pattern of MYD88 staining and immune infiltrates in the bone marrows of *MYD88* wild-type (*MYD88*^{WT}) and *MYD88*^{L265P} mice are recapitulated in the human setting, which provides insight into LPL/WM pathogenesis. Furthermore, histologic transformation to DLBCL is associated with acquisition of secondary genetic lesions frequently seen in de novo human DLBCL as well as LPL/WM-transformed cases. These findings indicate that, although the *MYD88*^{L265P} mutation might be indispensable for the LPL/WM phenotype, it is insufficient by itself to drive malignant transformation in B cells and relies on other, potentially targetable cooperating genetic events for full development of lymphoma.

Introduction

Recent studies using whole-genome sequencing have uncovered the genetic landscape of hematologic malignancies. Among the most common alterations is a gain-of-function mutation (L265P) in the *MYD88* gene, which is exceptionally high in lymphoplasmacytic lymphoma/Waldenström macroglobulinemia (LPL/WM; 90%-100%).[1-4] The *MYD88*^{L265P} mutation is highly prevalent in diffuse large B-cell lymphoma (DLBCL), particularly in a poor-prognosis molecular subtype of activated B-cell (ABC) DLBCL (50%) termed C5/MCD[5,6] and in extranodal variants of DLBCL.[7,8] Despite recent advances in treatment, LPL/WM and ABC DLBCL remain challenging clinical problems.[9,10] Therefore, there is an urgent need to better understand the molecular and cellular roles of the specific genetic lesions identified by high-throughput genetic analysis that drive lymphomagenesis.

The MYD88^{L265P} mutation leads to spontaneous assembly of a protein complex called the myddosome, which activates NF-κB signaling.[11-13] It was recently shown that in LPL/WM and DLBCL cells, MYD88

Submitted 18 June 2019; accepted 20 August 2019. DOI 10.1182/bloodadvances.2019000588.

*T.S. and M.L.G. contributed equally to this study.

SRA accession number is PRJNA560216, and the records can be found under https://www.ncbi.nlm.nih.gov/sra/PRJNA560216.

The full-text version of this article contains a data supplement.

and other components of the myddosome aggregate into a larger multiprotein complex with TLR9 and BCR called My-T-BCR.[14] Genetic or pharmacologic inhibition of MYD88^{L265P} signaling is toxic to LPL/WM and ABC DLBCL cells.[11,12] Although these findings rationalize the development of MYD88^{L265P}-targeted therapeutic strategies, the exact role of this mutated protein in lymphoma initiation, and its ability to promote neoplastic transformation, are still not fully understood.

Although a knockin model of the murine L252P mutation (corresponding to human L265P) developed a polyclonal lymphoproliferative disorder (LPD) that progressed to a BCL6^{-} DLBCL,[15] the long latency of DLBCL occurrence suggests acquisition of spontaneous cooperating mutations. Moreover, the LPD in the L252P model was described as "a largely monomorphic lymphoid cell population with indolent appearance," lacking the morphologic features of LPL/WM.[15] We generated transgenic mice expressing the human MYD88 wild-type (MYD88^{WT}) or MYD88^{L265P} protein in germinal center (GC) and post-GC B cells, primarily because of the above results, along with these 4 observations: (1) the high incidence of the L265P mutation in human LPL/WM,[1-4] (2) the structural differences between the human and mouse proteins,[16] (3) the lack of reports about spontaneous development of LPL/WM-like tumors in mice,[17] and (4) the potential utility of an animal model of human *MYD88*^{L265P} for targeted drug screens. Here, we show that the *MYD88*^{L265P} mutation (despite inducing downstream NF-κB p65 nuclear translocation) is insufficient to drive malignant transformation by itself, although it does promote a non-clonal, low-grade B-cell LPD with several clinicopathologic features resembling LPL/WM, which occasionally undergoes transformation to DLBCL harboring secondary mutations and expressing BCL6, as documented for human DLBCL cases transformed from LPL/WM.[18,19]

Materials and methods

Transgenic mice

Conditional *hMYD88*(*WT*)^{LSL} and *hMYD88*(*L265P*)^{LSL} transgenic mice were generated using a modified site-specific integration method,[20] in which the tetracycline-responsive promoter was replaced with a CAG promoter and lox-stop-lox (*LSL*) cassette.[21] Targeting vectors harboring the human *MYD88*^{WT} or *MYD88*^{L265P} complementary DNA downstream of the *LSL* cassette were electroporated together with an *Flp* recombinase-expressing plasmid into the C2 mouse embryonic stem cell line. Targeted integration of the *MYD88* gene at flippase recognition target sites downstream of the mouse *Col1A1* gene activated hygromycin resistance enabling selection. Positive clones were injected into C57BL/6 blastocysts, which gave rise to chimeras and eventually to transgenic mice. To remove the *LSL* cassette, *hMYD88* mice were crossed with those bearing *AID*^{Cre}.[22] All experiments were approved by the Institutional Animal Care and Use Committee (IACUC 05-065) of the Dana-Farber Cancer Institute.

Human samples

Archival paraffin-embedded bone marrow (BM) biopsies from patients with LPL/WM were obtained from the Pathology Department at Brigham and Women's Hospital. Use of human material was approved by the Dana-Farber Cancer Institute Institutional Review Board (IRB 01-206) in compliance with the Declaration of Helsinki.

Histopathology, immunohistochemistry (IHC), immunofluorescence, and immunoblotting

Histopathology, IHC, immunofluorescence, and immunoblotting analyses were performed according to standard protocols and manufacturers' recommendations. For details, see supplemental Materials and methods.

Flow cytometry and cell sorting

To induce T-cell–dependent B-cell responses and GC formation, which facilitated cell sorting and flow cytometry analysis in young animals, mice were immunized by intraperitoneal injection of 5×10^8 sheep red blood cells (Innovative Research, Novi, MI) in 200 μL of phosphate-buffered saline and analyzed 10 days later, as described.[23] Single-cell suspensions of mouse splenocytes or lymph node (LN) cells were isolated by pushing minced tissue through a strainer. Red blood cells were lysed, and leukocytes were stained with Zombie Aqua (BioLegend, San Diego, CA) and primary antibodies (supplemental Table 1) according to the manufacturer's recommendations. Cells were analyzed using an LSRFortessa flow cytometer (BD Biosciences, San Jose, CA) or fluorescence-activated cell sorted (FACS) using FACSAria II (BD Biosciences; gating indicated in Figure 2H). Flow cytometric data were analyzed using FlowJo software.

Polymerase chain reaction analysis, clonality assessment, and whole-exome sequencing

For polymerase chain reaction analysis of the *LSL* cassette deletion, DNA was isolated from cells sorted by using FACS with the AllPrep DNA/RNA Kit (Qiagen, Hilden, Germany), amplified using Q5 High-Fidelity DNA Polymerase (New England Biolabs, Ipswich, MA), separated on agarose gel, and visualized with a ChemiDoc MP imaging system (Bio-Rad Laboratories, Hercules, CA). DNA from LNs, spleens, tumors, liver, and tails was isolated using a Gentra Puregene kit (Qiagen). *MYD88* transgenes were sequenced using Sanger sequencing. *IgH* gene rearrangements for lymphoma clonality assessment were analyzed using Southern blotting as described.[24] Whole-exome sequencing was performed on 3 DLBCL and tail sample pairs as well as 1 tail sample from a healthy animal as an additional control. For details, see supplemental Materials and methods.

Serum protein electrophoresis and multiplex immunoassays

Serum was analyzed on SPIFE Serum Protein Gels with SPIFE 3000 gel electrophoresis (Helena Laboratories, Beaumont, TX). Mouse Magnetic Luminex Assay (R&D Systems, Minneapolis, MN), and Mouse Immunoglobulin Isotyping Magnetic Bead Panel (Millipore, Burlington, MA) kits were used to assess serum cytokines and immunoglobulin (Ig) concentrations, respectively, according to the manufacturers' protocols.

Results

Aicda-driven overexpression of MYD88^{L265P} induces abnormal inflammatory changes

To investigate the oncogenic potential of the somatic *MYD88*^{L265P} mutation, we cloned WT or L265P-mutated human *MYD88* complementary DNA sequences into the targeting vector (Figure 1A). Because both human LPL/WM and ABC DLBCL

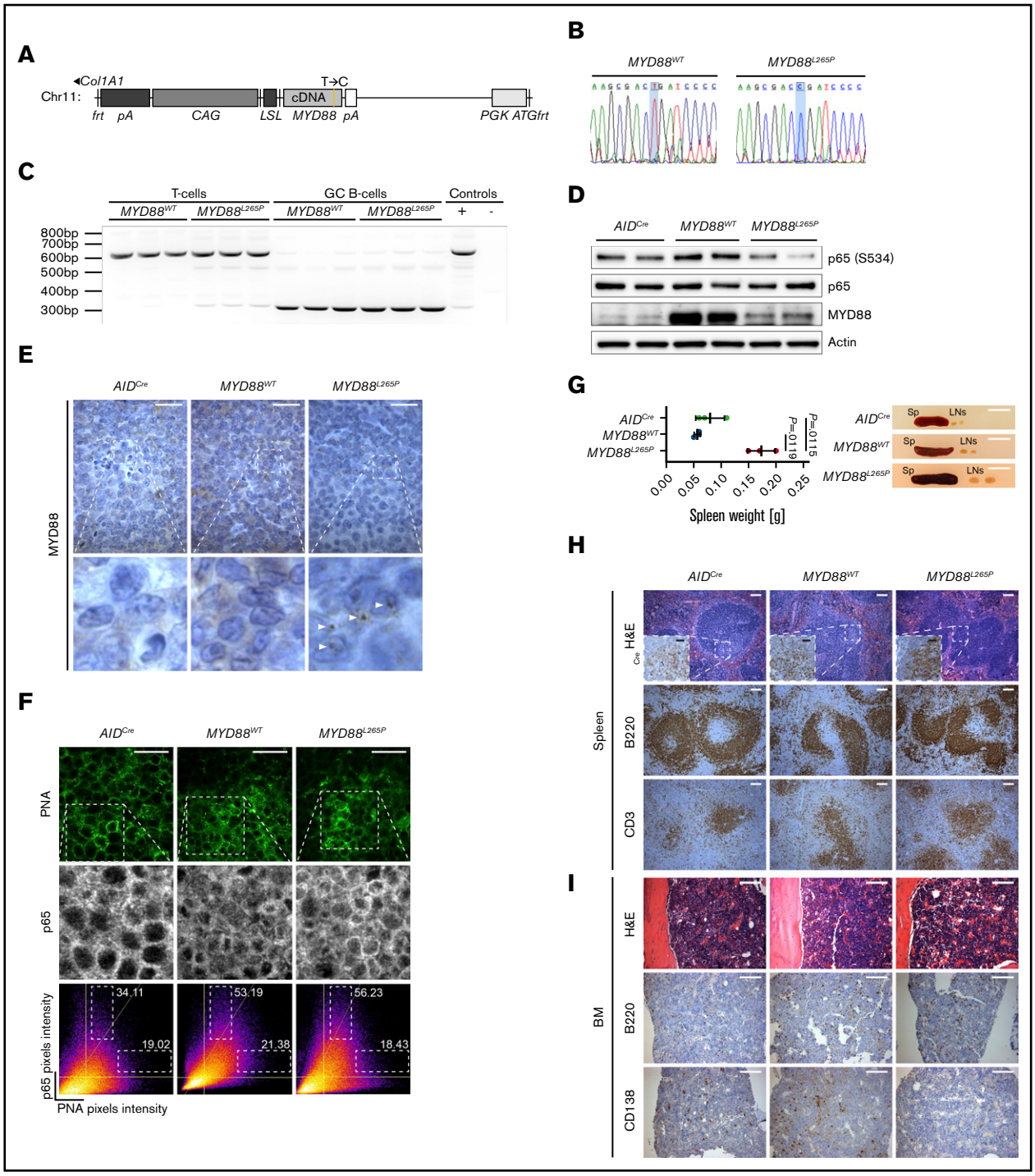

Figure 1. Generation and validation of conditional *hMYD88(L265P)*^{LSL} transgenic mouse model. (A) Schematic representation of the targeting vector integration site downstream of the mouse *Col1A1* gene that supports high transgene expression in a variety of cell types including B cells. WT or L265P-mutated human *MYD88* complementary DNA (cDNA) sequences were cloned into the targeting vector downstream of the *loxP*-flanked stop cassette (*LSL*) and electroporated together with an Flp recombinase-expressing plasmid into the C2 mouse embryonic stem cell line. C2 cells are engineered to acquire hygromycin resistance after targeted integration of the gene of interest at flippase recognition target (*frt*) sites. (B) Sanger sequencing of the human *MYD88* sequence amplified from splenic genomic DNA isolated from transgenic mice. The presence of T>C transition results in the L265P mutation in *MYD88*^{L265P} mice. (C) AID^{Cre}-induced deletion of the *LSL* cassette assessed by polymerase chain reaction (PCR) using primers indicated as arrows in panel A in FACS splenic T cells and GC B cells from *MYD88*^{WT} (n = 3) and *MYD88*^{L265P} (n = 3) mice immunized with sheep red blood cells (SRBCs). *loxP*-flanked sequence: 640 bp; deleted: 330 bp. (D) Immunoblot analysis of MYD88 protein expression and p65 (S534) phosphorylation in FACS splenic GC B cells from *AID*^{Cre} (n = 2), *MYD88*^{WT} (n = 2), and *MYD88*^{L265P} (n = 2) mice immunized with SRBCs relative to actin. (E) Immunohistochemical analysis of MYD88 expression within GCs of *AID*^{Cre}, *MYD88*^{WT}, and *MYD88*^{L265P} mice. GCs were identified based on morphology and the presence of apoptotic bodies as well as Ki-67 staining

originate from post-GC B cells,[25,26] we deleted the *LSL* stop cassette to overexpress human MYD88^{WT} or MYD88^{L265P}-mutated proteins in antigen-experienced B cells using *Aicda*-driven Cre recombinase. We achieved this by breeding *AID*$^{Cre/+}$*;MYD88(WT)*$^{LSL/-}$ and *AID*$^{Cre/+}$*;MYD88(L265P)*$^{LSL/-}$ mice, referred to as *MYD88*^{WT} and *MYD88*^{L265P}, respectively, and we used *AID*$^{Cre/+}$ mice (referred to as *AID*^{Cre}) as controls. We confirmed the presence of WT or L265P-mutated human *MYD88* transgene sequences in the spleens of both transgenic mice (Figure 1B).

Next, we evaluated the efficacy of *AID*^{Cre}-mediated induction of *MYD88* transgene expression and activity in vivo. We detected deletion of the *LSL* cassette in FACS GC B cells, but not T cells, from both *MYD88*^{WT} and *MYD88*^{L265P} mice (Figure 1C). MYD88 protein abundance consistently increased in GC B cells from both *MYD88*^{WT} and *MYD88*^{L265P} mice compared with *AID*^{Cre} mice (Figure 1D-E). However, expression of MYD88^{L265P} was lower than that of MYD88^{WT}, suggesting different maturation and/or reduced stability of the mutant protein. Moreover, we observed different patterns of subcellular distribution between the 2 forms. Although MYD88^{WT} was evenly distributed among the cells, MYD88^{L265P} was confined to small foci within mouse GC cells and transfected HEK293T cells, suggesting that the L265P mutation enhances oligomerization and resembles formation of myddosome/My-T-BCR[13,14] in vivo (Figure 1E; supplemental Figure 1A). We subsequently found that overexpression of both human MYD88^{L265P} and MYD88^{WT} enhanced nuclear localization of p65 in mouse GC B cells and transfected HEK293T cells (Figure 1F; supplemental Figure 1B-C). However, only the *MYD88*^{L265P} cells demonstrated decreased p65 (S534) phosphorylation (Figure 1D). Blockage of p65 (S534) phosphorylation was previously shown to increase p65 stability and enhance NF-κB–dependent gene expression,[27] suggesting different activities of mutated vs WT protein. These findings confirm that AID^{Cre} induces expression of human MYD88^{L265P}, resulting in activation of its downstream targets in murine GC B cells.

To initially assess the effect of *MYD88* transgene expression on development of lymphoid organs and B cells, we examined 8- to 16-week-old *AID*^{Cre}, *MYD88*^{WT}, or *MYD88*^{L265P} mice. Gross pathologic examination revealed moderately enlarged spleens in the *MYD88*^{L265P} compared with *AID*^{Cre} and *MYD88*^{WT} mice (Figure 1G). Conversely, no obvious histologic changes were observed in the spleens and BMs of *MYD88*^{L265P} mice compared with *AID*^{Cre} and *MYD88*^{WT} animals (Figure 1H-I). Immunostaining for B220 and CD3 showed normal B-cell:T-cell ratios in the spleens (Figure 1H). Likewise, there was no substantial increase in the number of B cells and CD138^{+} plasma cells in the BMs of *MYD88*^{L265P} compared with control mice (Figure 1I). These results show that expression of *MYD88*^{WT} and *MYD88*^{L265P} transgenes induce no major histopathologic changes during early development of lymphoid organs.

Starting at 8 weeks of age, however, 90% of *MYD88*^{L265P} mice, but none of the *AID*^{Cre} and *MYD88*^{WT} controls, began to develop skin rash and hair loss restricted to the submandibular areas, even as the mice aged (Figure 2A). We detected a mixed cellular infiltrate composed predominantly of T cells and histiocytes as well as scattered mast cells and B cells in the dermis of *MYD88*^{L265P} mice (Figure 2B-F). Furthermore, regional cervical LNs were found to be particularly enlarged when compared with other LNs in *MYD88*^{L265P} mice. This size change was caused by cystic formation vs an inflammatory response or lymphoproliferation only in the cervical LNs (Figure 2G).

To examine whether this focal dermal phenotype was associated with systemic alterations of immune cells, we immunized mice with sheep red blood cells to induce GC formation and measured lymphocyte subpopulations in the spleens using flow cytometry (Toll-like receptor agonists were not tested because they may blunt the differences between mice with and without the *MYD88*^{L265P} mutation). Significant differences in total numbers of T cells, B cells, and plasma cells were not observed, although the percentage of plasma cells was elevated in *MYD88*^{L265P} vs *AID*^{Cre} and *MYD88*^{WT} mice (Figure 2H-I). Increased numbers of plasma cells were also detected using IHC (supplemental Figure 1D).

Next, we performed a multiplex immunoassay on serum samples from *MYD88*^{L265P} mice divided into groups based on the severity of their skin lesions: group I contained mice with mild rash and alopecia, which did not progress or form major fibrosis over time, and group II contained mice whose skin lesions progressed to lip retraction and fibrosis. We found that *MYD88*^{L265P} mice in group II had significantly increased concentrations of IgM, IgG1, IgG2b, and IgG3, but not IgA, when compared with littermates in group I (Figure 2J). Accordingly, we evaluated systemic inflammation by measuring the abundance of interleukin-6 (IL-6), a major proinflammatory cytokine.[28] Higher IL-6 levels were present in the serum of group II compared with group I (Figure 2K). Moreover, we observed higher IL-6 abundance in mast and stromal cells in the dermis of *MYD88*^{L265P} compared with *MYD88*^{WT} mice (Figure 2L). Although CXCL13 serum levels did not correlate with the severity of skin lesions, its expression was locally increased in mast and stromal cell similar to that of IL-6 (Figure 2L). These findings show

Figure 1. (continued) in serial consecutive sections. Note punctate, cytoplasmic MYD88 staining in the *MYD88*^{L265P} (white arrowheads) but not *MYD88*^{WT} or *AID*^{Cre} mice. Scale bars, 20 μm (see also supplemental Figure 1A). (F) Immunofluorescence analysis of p65 (white) subcellular localization within GC B cells (peanut agglutinin [PNA]; green) in spleens from *AID*^{Cre}, *MYD88*^{WT}, and *MYD88*^{L265P} mice immunized with SRBCs (top and middle). Lower-magnification images (×40) were quantified using ImageJ (bottom). Gates were set up to quantify voxels with high intensity of p65 and low intensity of PNA staining or high intensity of PNA and low intensity of p65 staining. The numbers represent mean intensity of voxels within the gated region, which is proportional to the number of events gated. Note increased nuclear p65 staining (quantified as voxels positive for p65 and negative for PNA, which stain cell membrane) in the *MYD88*^{WT} and *MYD88*^{L265P} but not *AID*^{Cre} mice. Scale bars, 20 μm (see also supplemental Figure 1B-C). (G) Spleen weights in 8- to 16-week-old *AID*^{Cre}, *MYD88*^{WT}, and *MYD88*^{L265P} mice (n = 3 per group). Graphs depict the mean ± standard deviation (SD). *P* values were calculated by using Welch's *t* test (left). Representative gross pictures of spleens (Sp) and LNs are shown on the right. Scale bars, 1 cm. Histologic (hematoxylin and eosin [H&E]) and IHC stains of indicated cell markers on consecutive serial sections from spleens (H) and BMs (I) from representative 8- to 16-week-old *AID*^{Cre}, *MYD88*^{WT}, and *MYD88*^{L265P} mice. B220, B cells; CD3, T cells; CD138, plasma cells. Scale bars: white, 100 μm; black, 25 μm. *pA*, polyadenylation sequences; *CAG*, cytomegalovirus enhancer/chicken β-actin promoter; *PGK ATGfrt*, phosphoglycerate kinase 1 promoter followed by ATG initiation codon restoring hygromycin resistance gene expression.

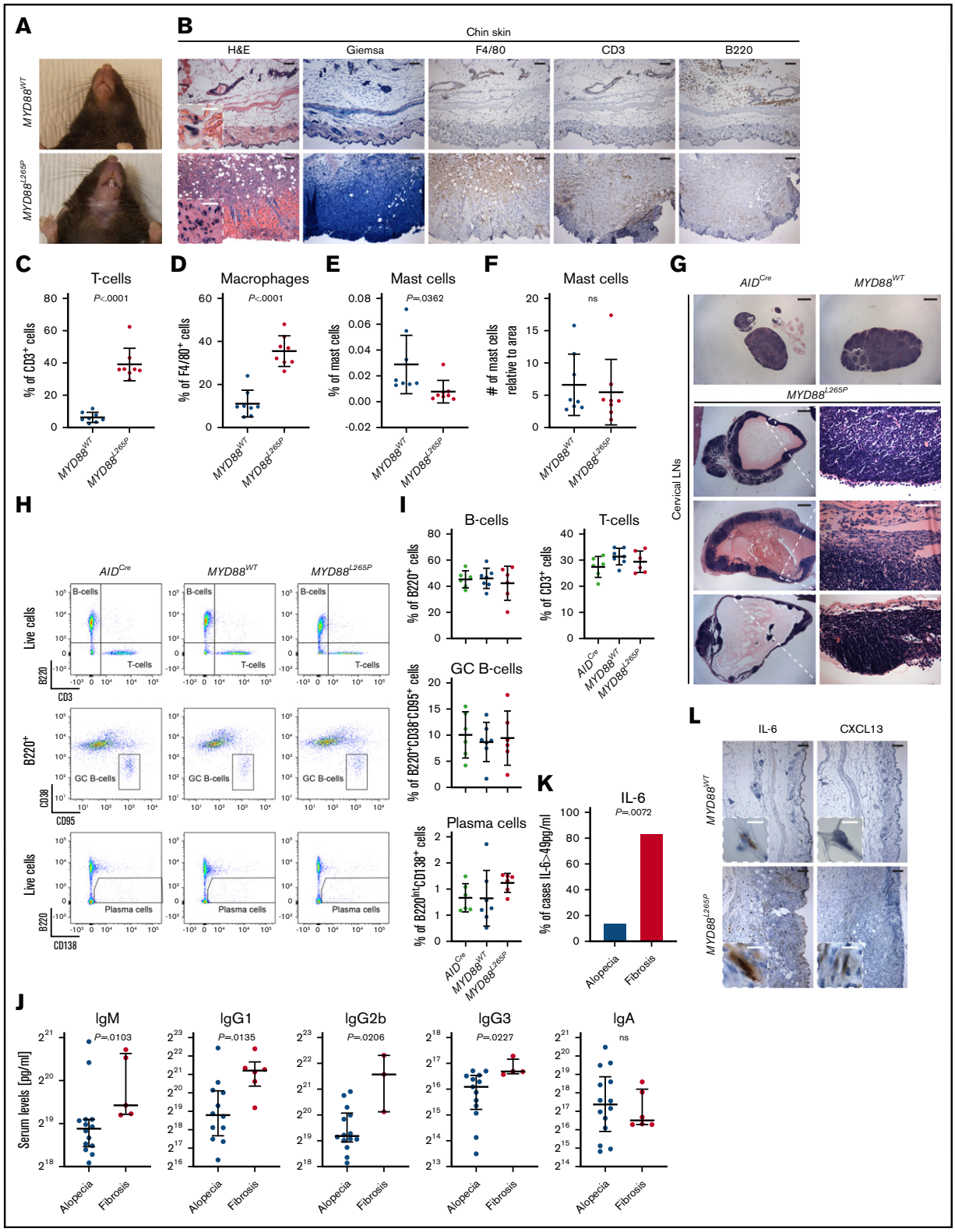

Figure 2. Skin, immune cell, and serum Ig changes in *MYD88*^{L265P} mice. (A) Representative gross pathology photographs of submandibular skin showing dermatitis and alopecia in *MYD88*^{L265P} but not *MYD88*^{WT} mice. (B) H&E, Giemsa, and IHC stains of indicated cell markers on serial submandibular skin sections from representative *MYD88*^{WT} and *MYD88*^{L265P} mice. Giemsa stain was used to identify mast cells; F4/80, macrophages. Scale bars: white, 10 μm; black, 100 μm. Percentage of T cells (C), macrophages (D), and mast cells (E) or number of mast cells relative to the tissue area (F) per field in the submandibular skin of *MYD88*^{WT} and *MYD88*^{L265P} mice. Measurements were made with inForm Cell Analysis Software analyzing 8 fields per genotype. Graphs depict the mean ± SD. *P* values were calculated by using Welch's

that neither skin lesions nor expression of *MYD88* transgenes in young animals induces conspicuous changes in the lymphoid organ B-cell:T-cell ratio or in GC response to acute activation. However, the focal skin changes are associated with systemic proinflammatory signaling in *MYD88*^{L265P} mice.

MYD88^{L265P} mice develop a low-grade, non-clonal LPD

To elucidate the role of MYD88^{L265P} protein in the pathogenesis of mature B-cell neoplasms, we evaluated *AID*^{Cre}, *MYD88*^{WT}, and *MYD88*^{L265P} mice over a 2-year aging period. Starting at 20 weeks, *MYD88*^{L265P} mice developed progressive lethargy, and by 67 weeks, 50% of the mice (11 of 22) had to be euthanized (Figure 3A). At autopsy, we observed a moderate splenic enlargement (not correlated with the severity of the submandibular skin lesions), along with generalized massive LN enlargement in 15 of 22 animals (Figure 3B-C); 33% of the mice exhibited macroscopic alterations consisting of lymphoid infiltrates in the liver and/or lungs (supplemental Figure 2A). Ill-defined white pulp and follicles, poorly demarcated from the reduced red pulp and interfollicular areas, were exclusively observed by histologic analysis in spleen and LNs from *MYD88*^{L265P} mice (Figure 3D-E). In line with the gross pathologic examination, LN architecture was more distorted than the splenic architecture. T-cell areas were mainly unaffected. In contrast, we noted an expansion of B220^{+}CD138^{DIM}CD5^{-} intermediate-size to large plasmacytoid cells, with greater expression of IgM relative to IgG and a low proliferation rate (5%-10% Ki-67^{+} cells) in *MYD88*^{L265P} compared with control mice (Figure 3D-E). No major infiltration of atypical cells was detected in the BMs of examined mice; however, a significant increase in the number of T cells, with an excess of CD8^{+} over CD4^{+} cells, and mast cells was observed in *MYD88*^{L265P} compared with age-matched control mice (Figure 3F; supplemental Figure 2B). Of note, plasmacytoid lymphocytes from *MYD88*^{L265P} mice showed the same focal pattern of MYD88 staining as the premalignant GC B cells (Figures 1E and 3E). No rearranged clonal bands for the *IgH* locus were detected by Southern blot analysis (Figure 3G), demonstrating that MYD88^{L265P} overexpression drives development of a premalignant, non-clonal, low-grade B-cell LPD with plasmacytic differentiation.

Analysis of LNs using flow cytometry did not reveal any significant differences in the number of total B cells between *MYD88*^{L265P} LPD mice and *AID*^{Cre} or *MYD88*^{WT} controls (Figure 4A). However, we detected significant expansion of GC B cells in *MYD88*^{L265P} LPDs compared with *AID*^{Cre} and *MYD88*^{WT} mice (Figure 4A). Moreover, the percentage of plasma cells was increased in *MYD88*^{L265P} LPDs compared with those in *AID*^{Cre} mice (Figure 4A). These findings suggest that although MYD88^{L265P} overexpression might not stimulate transient B-cell activation, its chronic, long-term signaling promotes progressive expansion of GC B cells over time.

Because LPL/WM is characterized by IgM gammopathy and the *MYD88*^{L265P} LPD cells had a large excess of IgM, we examined the serum proteins of the mice by electrophoresis. In line with the previous findings, we detected diffuse bands, indicating a polyclonal increase in gamma globulins in *MYD88*^{L265P} compared with *AID*^{Cre} and *MYD88*^{WT} mice (Figure 4B). Moreover, multiplex immunoassay revealed that serum concentrations of IgM, but not IgG1, IgG3, or IgA, were significantly higher in *MYD88*^{L265P} compared with controls (Figure 4C; supplemental Figure 2C). IgG2b concentration was significantly increased in *MYD88*^{L265P} compared with *MYD88*^{WT} mice and showed a positive correlation with IgM concentrations ($r = 0.7373$; supplemental Figure 2C-D). Rouleaux formation was subsequently detected in stains of peripheral blood smears (Figure 4D).

Given the focal skin lesions in *MYD88*^{L265P} mice, as well as the increase in proinflammatory cytokine secretion in LPL/WM patients,[29] we examined serum IL-6 abundance and found higher concentrations in *MYD88*^{L265P} vs *AID*^{Cre} and *MYD88*^{WT} mice (Figure 4E). Furthermore, we detected a higher concentration of CXCL13 (a B-cell chemoattractant that is elevated in LPL/WM patients)[30] in the serum of *MYD88*^{L265P} mice with macroscopic lung or liver lymphoid infiltrates at autopsy in comparison with other groups (Figure 4F). Taken together, these findings show that *MYD88*^{L265P} mice develop a non-clonal, B-cell lymphoproliferation with certain characteristic features of LPL/WM, such as plasmacytic differentiation, increased IgM levels, rouleaux formation, and proinflammatory signaling.

With longer latency, *MYD88*^{L265P} mice acquire secondary genetic lesions and develop clonal high-grade B-cell lymphoma

During the aging period, specifically at older ages (median of 85.8 weeks vs 56.3 weeks for LPD), 4 of 22 *MYD88*^{L265P} mice developed a more aggressive disease characterized by massive enlargement of spleen and LNs (Figure 5A). Focal skin lesions were limited to a mild rash in these animals. Therefore, we examined the lymphoid organs by histology, IHC, and flow cytometry. Tissue architecture was distorted by a diffuse infiltrate of medium-size to large B220^{+}BCL6^{+}CD138^{-}CD5^{-} cells with a high proliferation rate (40%-80% Ki-67^{+} cells). The cells were admixed with residual CD138^{+} plasmacytoid cells (Figure 5B-C). In addition, the neoplastic cells infiltrated other organs, including kidney, liver, lung, and BM (data not shown; Figure 5B; supplemental Figure 2A). Small focal infiltrates were also detected in the brains and at the outer meninges (data not shown). Southern blot analysis of the *IgH* gene locus revealed that the neoplasms were clonal (Figure 5D).

Figure 2. (continued) *t* test. (G) Histologic (H&E) analysis of representative cervical LNs demonstrating cyst development in *MYD88*^{L265P} but not in *AID*^{Cre} or *MYD88*^{WT} mice. Scale bars: white, 50 μm; black, 500 μm. Representative density plots (H) and graphs (I) depicting the mean ± SD of flow cytometric analysis of splenic lymphoid cell subpopulations from *AID*^{Cre} (n = 6), *MYD88*^{WT} (n = 7), and *MYD88*^{L265P} (n = 6) mice immunized with SRBCs. (J) Serum Ig concentrations assessed using multiplex immunoassay in *MYD88*^{L265P} mice grouped according to severity of submandibular skin lesions. Graphs depict the median ± 25th to 75th percentile. *P* values were calculated by using Mann-Whitney *U* test. (K) Percentage of *MYD88*^{L265P} mice classified by the severity of submandibular skin lesions with serum IL-6 concentrations >49 pg/mL assessed using multiplex immunoassay. *P* value was calculated by using Fisher's exact test. (L) IHC stains of indicated cytokines on serial submandibular skin sections from representative *MYD88*^{WT} and *MYD88*^{L265P} mice. Scale bars: white, 10 μm; black, 100 μm.

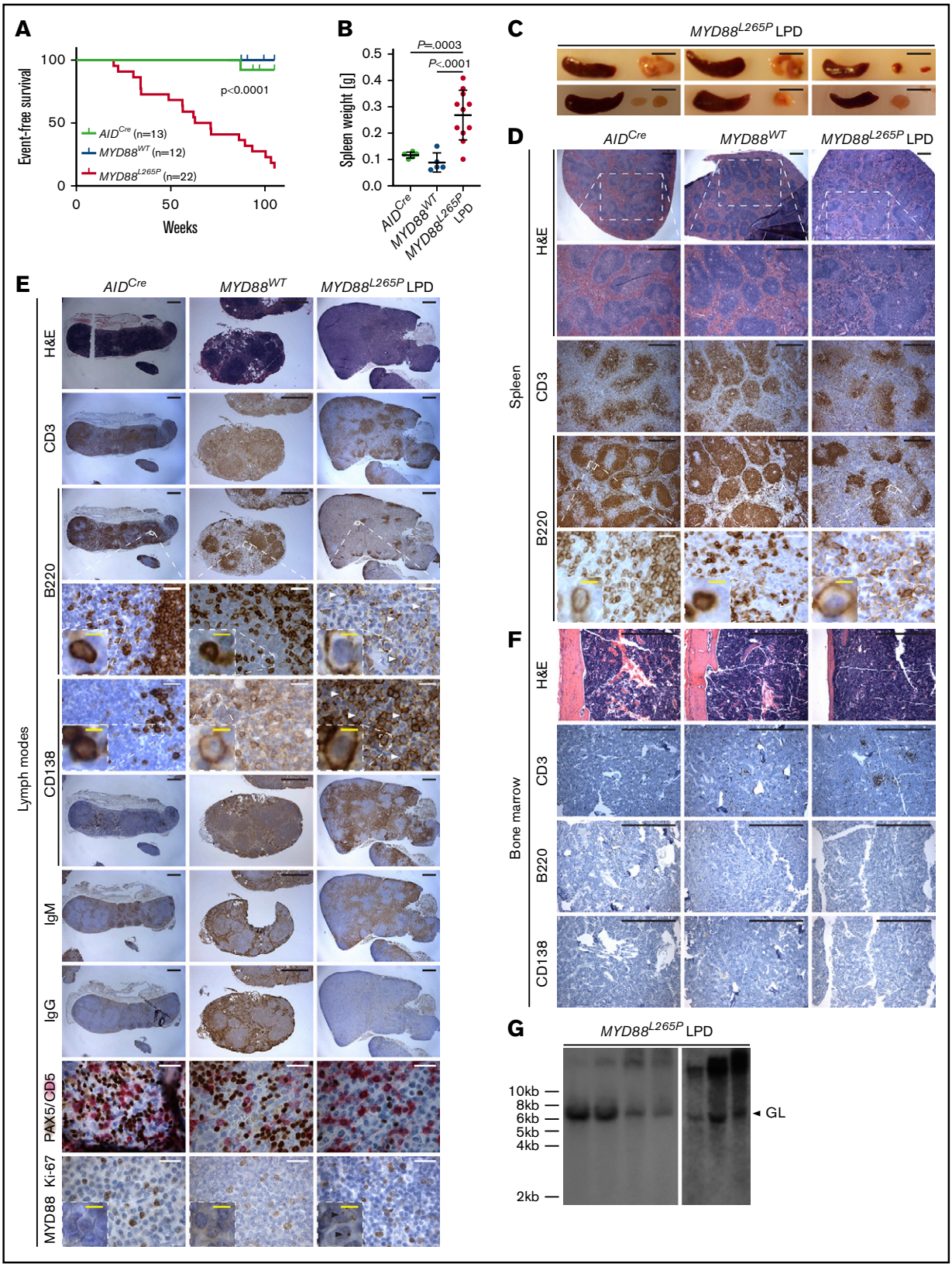

Figure 3. Development of a non-clonal, low-grade B-cell LPD in *MYD88*^{L265P} mice. (A) Kaplan-Meier plots illustrating event-free survival of aging cohorts of *AID*^{Cre} (n = 13), *MYD88*^{WT} (n = 12), and *MYD88*^{L265P} (n = 28) mice. *P* value was calculated by using a log-rank test. (B) Spleen weights in aged *AID*^{Cre} (n = 5) and *MYD88*^{WT} (n = 5) control mice and *MYD88*^{L265P} (n = 11) mice with LPD. Graphs depict the mean ± SD. *P* values were calculated by using Welch's *t* test. (C) Gross images of spleens and LNs from representative *MYD88*^{L265P} mice with low-grade B-cell LPD. Scale bar, 1 cm. Histologic and IHC stains of indicated markers on serial spleen (D), LN (E), and

Large B cells showed a focal pattern of MYD88 immunostaining, indicating its continuous activation in these transformed cells. We also detected higher concentrations of serum CXCL13 in the high-grade cases compared with the other *MYD88*^{L265P} ($P = .0091$), *MYD88*^{WT} ($P = .0238$), and *AID*^{Cre} ($P = .0167$) mice (Figure 4F). These observations were consistent with the clinicopathologic diagnosis of DLBCL in human patients.

The prominent lymphoplasmacytic infiltrate, longer latency, and BCL6 expression[18,19] suggested that these neoplasms might have arisen from the LPD by acquiring cooperative genetic alterations. We therefore performed whole-exome sequencing of 3 *MYD88*^{L265P} DLBCLs and detected an average of 216 single nucleotide variants and 49 indels per sample (supplemental Table 2). Remarkably, somatic variants involved genes that are frequently mutated and/or constitute pathways perturbed in human DLBCLs, including some related to MYD88/NF-κB and BCR signaling.[5,6] For several of these genes, which included *Malt1*, *Klf2*, *Gna13*, *Dusp2*, *Pik3c2g*, *Pdgfrb*, and *Pim1,* the location and impact of the mutations closely mirrored mutations documented in human DLBCL (Table 1). Two of 3 samples had *Pim1* mutations (Figure 5E) and mutations in other genes targeted by aberrant somatic hypermutation.[6] Taken together, these results point out potential secondary genetic lesions cooperating with *MYD88*^{L265P}-promoted clonal lymphomagenesis and suggest that our *MYD88*^{L265P} model recapitulates pathogenetic events observed in human DLBCL.

MYD88^{L265P} leads to formation of protein aggregates and increases BM immune infiltration in LPL/WM patients

The focal pattern of MYD88 staining selectively observed in *MYD88*^{L265P} cells prompted us to investigate whether it would enable differentiation of LPL/WM patients according to *MYD88* mutations; especially since the presence of similar structures was recently shown to be a predictive marker in DLBCL.[14] We found that plasmacytoid lymphocytes in BM biopsies from LPL/WM patients with *MYD88*^{L265P} ($n = 13$) expressed a higher amount of MYD88 protein aggregated in focal structures when compared with *MYD88*^{WT} patients ($n = 11$) (Figure 6A). This suggests that MYD88 immunostaining may be a useful diagnostic marker for detection of MYD88^{L265P} mutation. However, this result needs to be validated in a much larger number of samples.

Finally, we evaluated the extent of T-cell and mast cell infiltration of BM biopsies from LPL/WM patients, given the increased immune infiltrates observed in BMs from *MYD88*^{L265P} mice (Figure 3F; supplemental Figure 2B). Consistent with the murine findings, we detected significantly higher T-cell and mast cell density in BMs from *MYD88*^{L265P} WM patients as compared with those in *MYD88*^{WT} patients (Figure 6B-E), suggesting that aberrant MYD88 signaling may promote their migration into the BM niche. Notably, we observed lower lymphoplasmacytic involvement in BMs of *MYD88*^{WT} compared with *MYD88*^{L265P} cases. Taken together, these results demonstrate that the murine *MYD88*^{L265P} model recapitulates many of the clinicopathologic features observed in human LPL/WM and DLBCL patients and provides a valuable resource for uncovering the pathogenesis of mutated MYD88.

Discussion

In this study, we demonstrated that AID^{Cre}-driven somatic activation of the *MYD88*^{L265P}, but not the *MYD88*^{WT}, transgene promotes a focal skin rash associated with increased systemic IL-6 signaling. With time, the majority of *MYD88*^{L265P} mice develop a premalignant, non-clonal, low-grade LPD with clinicopathologic features resembling LPL/WM and progressing, albeit at low frequency, to clonal, high-grade DLBCL in aged mice. Recapitulation of the murine findings in the human setting corroborates their similarity and provides clinical correlations and insight into the pathogenesis of LPL/WM.

The exceptionally high prevalence of the *MYD88*^{L265P} mutation in human LPL/WM indicates its important role in these neoplastic cells. However, the exact mechanism of action and whether it is sufficient to drive LPL/WM pathogenesis need clarification. Our findings showed that although human *MYD88*^{L265P} alone is insufficient to induce full-blown LPL/WM neoplasia, it does foster emergence of LPL/WM-specific clinicopathologic features, including expansion of lymphoplasmacytic cells, elevated serum IgM concentration, rouleaux formation (which can be caused by increased Ig levels or inflammation),[31] increased number of T- and mast cells in the BM, and proinflammatory cytokine signaling, the latter representing an integral part of LPL/WM pathogenesis. Personal and family history of chronic autoimmune and inflammatory conditions significantly correlate with the risk of developing LPL/WM.[32,33] Development of skin lesions and LN cysts specifically in the submandibular area of *MYD88*^{L265P} mice colocalize with squamous papillomas reported in *AID*$^{Cre/+}$;*Pten*$^{lox/lox}$ mice, suggesting that the changes are triggered by *Aicda*-driven activation of the transgene in non-lymphoid cells.[34] Likewise, a germline-activating mutation of the *MYD88* gene was recently described in a patient with skin rash, severe arthritis, and elevated serum IL-6 concentration.[35] Moreover, despite the lack of lymphoplasmacytic infiltrate in the BM of *MYD88*^{L265P} mice with LPD, MYD88^{L265P}-driven systemic proinflammatory signaling may mediate remodeling of the BM niche, leading to increased numbers of T cells and mast cells. Notably, clonal expansion of cytotoxic T cells was reported in blood samples from LPL/WM patients[36] and could contribute to better clinical responses of *MYD88*^{L265P} patients.[37] IL-6 signaling was also shown to mediate IgM secretion in WM cells.[38] Altogether, these focal and systemic inflammatory changes may predispose *MYD88*^{L265P} mice to develop the LPL/WM-like LPD phenotype.

Although LPL/WM and DLBCL cells harboring the *MYD88*^{L265P} mutation depend on its activity,[11,12] little is known about the role of *MYD88*^{L265P} in tumor initiation in the context of intact tumor suppressors and no additional genetic alterations. In keeping with our results, overexpression of *MYD88*^{WT} was shown to suffice for NF-κB activation.[39] However, when introduced into primary mouse

Figure 3. (continued) BM (F) sections from representative, age-matched *AID*^{Cre} and *MYD88*^{WT} control mice, and 1 *MYD88*^{L265P} mouse with LPD. Note expansion of plasmacytoid lymphocytes (white arrowheads) in the *MYD88*^{L265P} mice compared with controls; and punctate, cytoplasmic MYD88 staining in the *MYD88*^{L265P} LPD cells (black arrowheads). Scale bars: white, 50 μm; black, 500 μm; yellow, 5 μm (see also supplemental Figure 2B). (G) Clonality evaluated by Southern blot analysis of the *IgH* gene in DNA isolated from LNs of *MYD88*^{L265P} ($n = 7$) mice with LPD. GL, non-rearranged germline band.

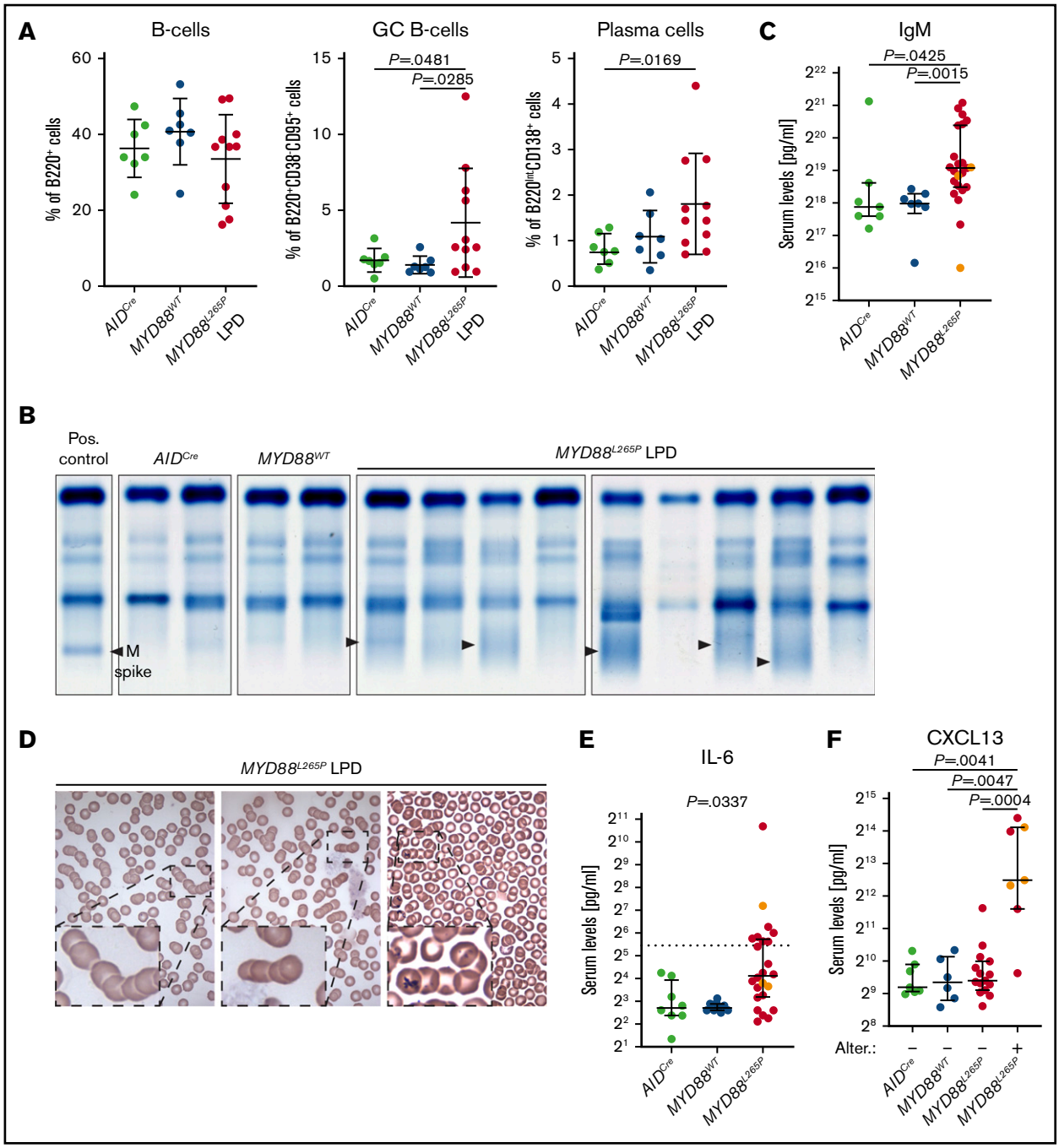

Figure 4. LPL/WM features of LPD in *MYD88*^{L265P} mice. (A) Flow cytometric analysis of lymphocyte subpopulations in LNs from aged *AID*^{Cre} (n = 7) and *MYD88*^{WT} (n = 7) control mice and *MYD88*^{L265P} (n = 11) mice with LPD. Graphs depict the mean ± SD. *P* values were calculated by using Welch's *t* test. (B) Serum protein electrophoresis of aged *AID*^{Cre} (n = 2) and *MYD88*^{WT} (n = 2) control mice and of *MYD88*^{L265P} (n = 9) mice with LPD. Note increased abundance of diffuse gamma globulins (black arrowheads) in *MYD88*^{L265P} mice compared with controls. A positive (Pos.) control containing a sharp band of gamma globulins (M spike) is shown for comparison. (C) Serum IgM concentrations assessed using multiplex immunoassay in aged *AID*^{Cre} (n = 7), *MYD88*^{WT} (n = 7), and *MYD88*^{L265P} (n = 23) mice. Orange points represent DLBCL animals in the *MYD88*^{L265P} cohort. Graphs depict the median ± 25th to 75th percentile. *P* values were calculated by using the Mann-Whitney *U* test (see also supplemental Figure 2C). (D) Peripheral blood smears demonstrating rouleaux formation of red blood cells in representative *MYD88*^{L265P} (n = 3) mice with LPD. (E) Serum IL-6 concentrations assessed by multiplex immunoassay in aged *AID*^{Cre} (n = 8), *MYD88*^{WT} (n = 8), and *MYD88*^{L265P} (n = 24) mice. Orange points represent DLBCL animals in the *MYD88*^{L265P} cohort; the dotted line indicates the assay sensitivity threshold. Graphs depict the median ± 25th to 75th percentile. *P* value was calculated by using Fisher's exact test. *P* value for the analysis with DLBCL samples omitted is .0491. (F) Serum CXCL13 concentrations assessed by multiplex immunoassay in aged *AID*^{Cre} (n = 7), *MYD88*^{WT} (n = 6), and *MYD88*^{L265P} mice with (n = 7) or without (n = 15) macroscopic liver and/or lung changes. Orange points represent DLBCL animals in the *MYD88*^{L265P} cohort. Graphs depict the median ± 25th to 75th percentile. *P* values were calculated by using the Mann-Whitney *U* test. *P* values for the analysis with DLBCL samples omitted are .0424, .0381, and .0139 for comparison of *MYD88*^{L265P} mice with macroscopic liver and/or lung changes with *AID*^{Cre}, *MYD88*^{WT}, and *MYD88*^{L265P} mice without macroscopic liver and/or lung changes, respectively (see also supplemental Figure 2A). Alter., alterations.

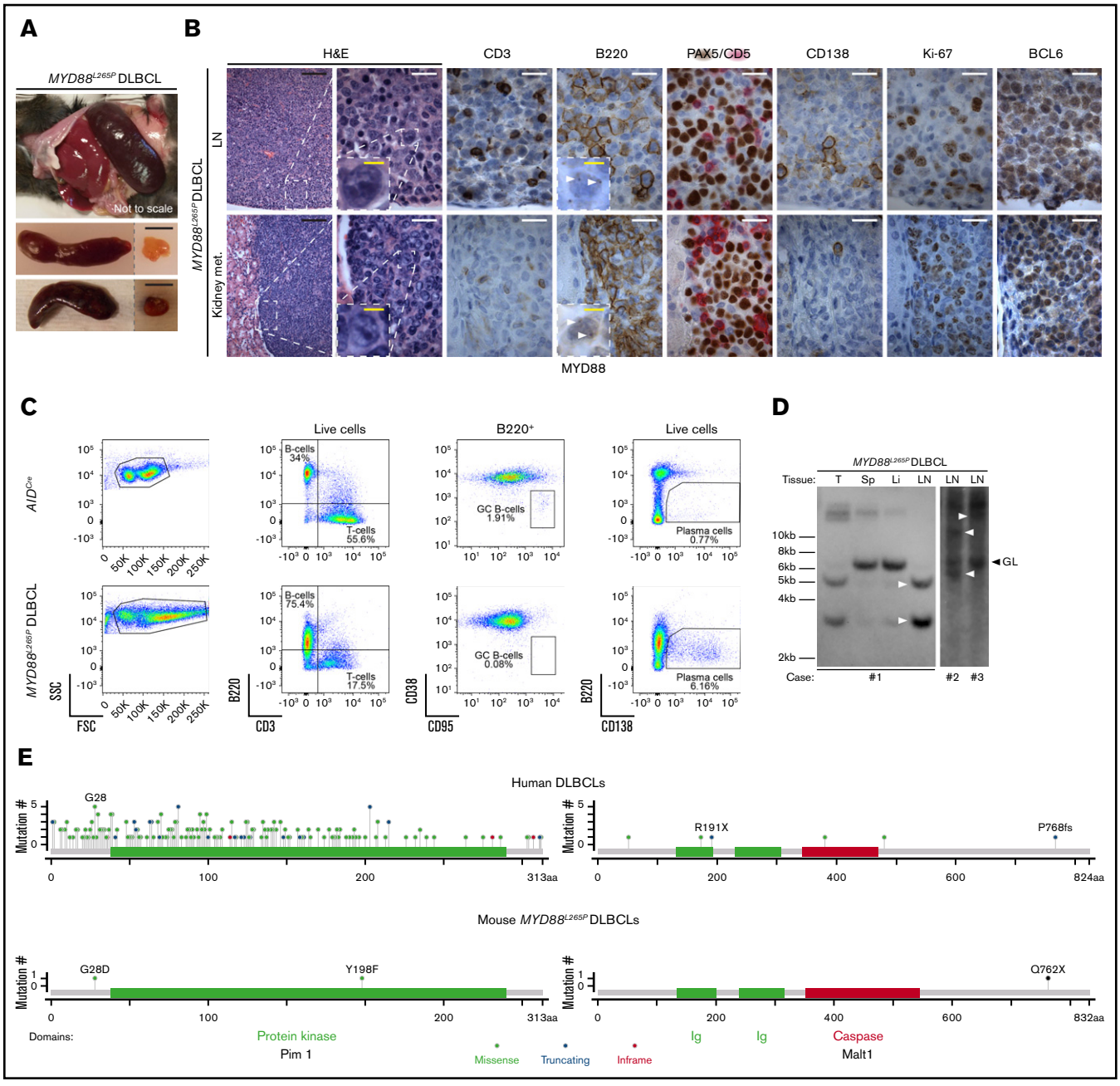

Figure 5. Development of DLBCL in *MYD88*^{L265P} mice. (A) Gross pathology images of spleens (top, in situ; bottom, dissected) and LNs from *MYD88*^{L265P} mice with DLBCL. Scale bars, 1 cm. (B) Histologic and IHC stains of indicated markers on serial LN (top) and kidney metastasis (met.) (bottom) sections from *MYD88*^{L265P} mice (n = 2) with DLBCL. Note punctate cytoplasmic MYD88 staining in the lymphoma cells (white arrowheads). Scale bars: white, 20 μm; black, 100 μm; yellow, 5 μm. (C) Density plots of flow cytometric analysis of indicated lymphocyte subpopulations in LNs from representative, age-matched *AID*^{Cre} control and *MYD88*^{L265P} DLBCL mice. (D) Clonality evaluated by Southern blot analysis of the *IgH* gene in DNA isolated from LNs, spleen (Sp), liver (Li), and tumor (T) of *MYD88*^{L265P} (n = 3) mice with DLBCL. Clonal rearranged bands are indicated with white arrowheads. (E) Location of murine *MYD88*^{L265P} and corresponding human DLBCL[6] somatic mutations in affected proteins.

B cells, only *MYD88*^{L265P}, but not *MYD88*^{WT}, downregulates p65 (S534) phosphorylation and induces NF-κB–dependent negative feedback mechanisms.[40] In contrast to prevailing assumptions, p65 (S534) phosphorylation is not required for p65 nuclear translocation.[27] Moreover, its blockage was shown to increase NF-κB–dependent transcription, at least toward certain target genes.[27] The biochemical properties of the MYD88^{L265P} protein also differ from the MYD88^{WT} protein in terms of stability[41] and the tendency to promote aggregation into complexes resembling myddosome/My-T-BCR.[13,14] The molecular differences between MYD88^{L265P} and MYD88^{WT} are consistent with the remarkably diverse phenotypic properties of MYD88 variants and suggest that *MYD88*^{L265P}-driven activity may well extend beyond the canonical MYD88 pathway.

Table 1. Human DLBCL-related somatic variants detected in mouse *MYD88*^{L265P} DLBCLs

	Mouse		Human			Notes	
Gene	Residue*	Domain	Downstream residue†	Upstream residue†	Domain	aSHM‡	Mouse
Bclaf1	Q18E	—	—	—	—	—	#2
Dusp2	L89V (L85)	Rhodanese	V66I	A96V/T	Rhodanese	Known	#2
			L67F	A99V/T/fs			
			L76P	E100D			
			E84D	L101P/F			
				P103L			
Gna13	R166Q	G-α	L152F	E167D	G-α	—	#1
			R166X	Q169H/X			
				V174E			
				F177S			
				L181X			
Klf2	G35D (G36)	—	E31D	N42D	—	Predicted	#3
			P32L/S	S43N			
			G36D				
Malt1	Q762X (Q754)	—	**P768fs**	**R191X**	—	—	#1
Pdgfrb	V567A (V568)	Cytoplasmic	—	—	—	—	#2
Pik3c2a	K391T (K390)	—	—	—	—	—	#2
Pim1	G28D	—	T23I	K29N	—	Known	#2
			K24N	E30K/D/Q/fs			
			L25V/M	K31R			
			A26P/T	E32K/Q/fs			
			P27S	P33S/T			
			G28D/A/D				
	Y198F	Kinase	L192V	D200N/H	Kinase		#3
			L193F/V	G203E/R			
			K194N	V206M/fs			
			T196I/S	Y207F			
			V197I	S208G/R/T			

*Human homolog residues are shown in parenthesis in case of heterogeneity.

†Up to 5 missense or truncating mutations 20 amino acids downstream and upstream of the residue altered in mouse *MYD88*^{L265P} DLBCLs. For *MALT1*, functionally related mutations are shown. Bold font indicates corresponding residues altered in mouse *MYD88*^{L265P} and human DLBCLs or having the same effect in the case of *Malt1*. Based on Chapuy et al,[5] Schmitz et al,[6] and Reddy et al.[54]

‡Aberrant somatic hypermutation (aSHM), according to Schmitz et al.[6]

In line with our findings, it was recently reported that a knockin mouse model carrying the endogenous mouse *Myd88*^{L252P} mutation developed LPD and DLBCL at a low frequency with considerably long latency.[15] However, the in vivo oncogenic activity of human and mouse MYD88 mutations seem to differ, which expands the knowledge about this highly recurrent mutation. The LPL/WM-like features of human *MYD88*^{L265P} LPD are not evident for the mouse *Myd88*^{L252P} LPD phenotype. Moreover, the mouse *Myd88*^{L252P} LPD had a high proliferation rate similar to that of DLBCL, contrary to human *MYD88*^{L265P} LPD, which was consistent with the low-grade LPL/WM-like phenotype. In contrast to our and others' results,[40] the published knockin *Myd88*^{L252P} model documented increased p65 (S534) phosphorylation, although it should be noted that these results were obtained in mouse embryonic fibroblasts rather than in B cells and thus may not be physiologically relevant or comparable to our results. No inflammatory changes were reported when expression of the mutant *Myd88*^{L252P} gene was induced by AID^{Cre}. Moreover, DLBCL cells in the mouse *Myd88*^{L252P} model were BCL6^{-}, especially when the animals were crossed with BCL2-overexpressing mice. This suggests that these lymphomas developed independently of LPD, because transformed human DLBCLs derived from LPL/WM, in contrast to de novo ABC DLBCLs, are generally BCL6^{+}.[18,19] In a different study, it was reported that *BCL2*$^{+/-}$*IL6*$^{+/-}$*AID*$^{-/-}$ mice develop an LPD-mimicking LPL/WM; however, the disease was also polyclonal and transcriptionally resembled chronic lymphocytic leukemia more than WM.[42] Moreover, IgM expression was artificially induced in this model by knocking out both alleles of *AID*, an enzyme that plays crucial roles in class-switching but is unaltered in tumor cells from LPL/WM patients.[42] Even though these models provide new insight into the pathogenesis of LPL/WM and DLBCL, a bona fide and clinically relevant murine model of human LPL/WM does not yet seem to exist.

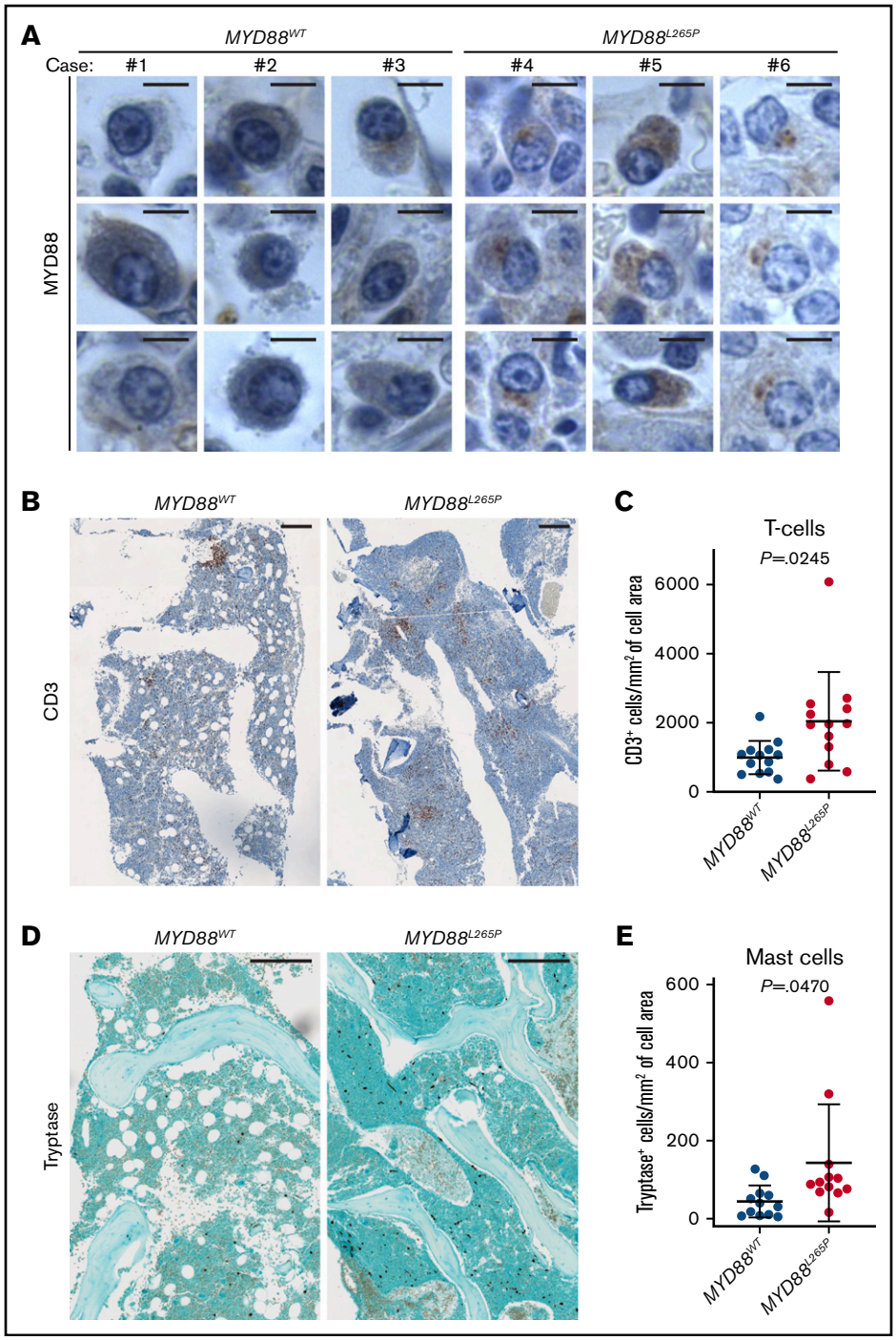

Figure 6. Implications of *MYD88*^{L265P} murine model for human LPL/WM. (A) MYD88 expression in plasmacytoid lymphocytes in BM biopsies from LPL/WM patients without (n = 11) and with (n = 13) *MYD88*^{L265P} mutation as evaluated by IHC staining. Three representative examples per each group are shown. Note punctate cytoplasmic staining of the MYD88^{L265P}, but not WT, protein. Scale bars, 5 μm. T-cell infiltration of BM biopsies from LPL/WM patients without (n = 13) and with (n = 13) the *MYD88*^{L265P} mutation. Representative IHC stains (B) and graphs (C) depicting the mean ± SD number of CD3$^+$ T cells per cell annotated area (mm^2) measured with HALO Image Analysis Software. Scale bars, 250 μm. *P* value was calculated by using Welch's *t* test. Mast cell infiltration of BM biopsies from LPL/WM patients without (n = 12) and with (n = 12) the *MYD88*^{L265P} mutation. Representative IHC stains (D) and graphs (E) depicting the mean ± SD number of tryptase$^+$ mast cells per cell annotated area (mm^2) measured with HALO Image Analysis Software. Scale bars, 250 μm. *P* value was calculated by using Welch's *t* test.

The non-clonal nature of the human *MYD88*^{L265P}-induced LPD, together with the acquisition of spontaneous secondary DLBCL-characteristic genetic lesions during clonal transformation to DLBCL, suggest that cooperating genetic alterations are required for *MYD88*^{L265P}-driven malignant transformation. Identification of such lesions, which may not be essential for normal cell survival, could facilitate therapeutic targeting of synthetic lethal interactions in *MYD88*^{L265P}-driven neoplasms, necessitated by inferior prognosis of DLBCL-transformed LPL/WM patients compared with de novo DLBCLs.[43] Thus, our model seems suitable for studying molecular pathogenesis of LPL/WM by crossing with animals bearing other mutations identified by our and by others' genomic analyses.[5,6,44] Accordingly, almost all *MYD88*^{L265P} LPL/WM patients show chromosome 6q14.1-6q27 deletions or *CXCR4* mutations.[45] Notably, both events are rare in *MYD88*^{WT} patients and result in downregulation of MYD88^{L265P}-induced tumor suppressor signaling.[45,46] In C5/MCD DLBCL, clonal *MYD88*^{L265P} mutations are associated with activating mutations of *CD79B*, which encodes a component of the BCR.[5,6] Expansion of mouse GC B cells in a germ-free environment indicates that human

MYD88^{L265P} may promote selection for self-antigens and thus activation of BCR signaling, which is dysregulated in both LPL/WM and DLBCL.[5,47] Importantly, engagement of the BCR upregulates Pim1 levels,[48] whose locus is frequently altered in C5/MCD cases[6] and during transformation from LPL/WM to DLBCL.[49] Pim1 kinase activates NF-κB signaling, enhances B-cell lymphomagenesis in vivo, and was shown to be a promising therapeutic target in ABC DLBCLs.[50-53] Of note, the C5/MCD subtype has the highest rate of aberrant somatic hypermutation compared with other DLBCLs.[5] Therefore, expression of a single human *MYD88*^{L265P} mutation (an early clonal event in human C5/MCD DLBCL) in activated mouse B cells induces selective pressure on secondary signaling and genomic alterations resembling human DLBCL pathogenesis.

Although its relatively long latency still precludes the use of our model for preclinical drug testing, the availability of this human transgene should facilitate the screening of MYD88-targeted therapeutics once a more rapidly tumorigenic model is created by genetic engineering. Moreover, *MYD88*^{WT} mice can serve to differentially screen for drugs that bind with greater specificity to the mutant protein, thereby enabling identification of less toxic compounds. In summary, human *MYD88*^{L265P} in transgenic mice promotes the development of a premalignant, non-lonal LPL/WM-like LPD with potential to transform to DLBCL in aged mice by acquiring secondary cooperating genetic alterations.

Acknowledgments

The authors thank Clyde Bongo and Madison L. O'Donnell of the Dana-Farber Cancer Institute (DFCI) Molecular Pathology Core Laboratory for help with imaging analyses, and members of the DFCI Flow Cytometry Core for assistance with cell sorting.

This work was supported by research grants from the Leukemia Lymphoma Society, the International Waldenstrom's Macroglobulinemia Foundation, the Waldenstrom's Macroglobulinemia Foundation of Canada, and a grant from the National Institutes of Health, National Cancer Institute (R01CA196783).

Authorship

Contribution: T.S., G.Y., S.P.T., and R.D.C. designed the research; T.S., M.L.G., K.A., P.S.D., K.W., Y.H., H.T., M.J., A.K., A.D., N.A.P., A.N., and M.G.D. performed the research; V.S., G.S.P., P.J., N.C.M., and S.P.T. contributed vital new agents or analytical tools; T.S., M.L.G., G.Y., Z.R.H., and R.D.C. analyzed data; and T.S. and R.D.C. wrote the article.

Conflict-of-interest disclosure: The authors declare no competing financial interests.

ORCID profiles: T.S., 0000-0003-4603-8517; M.J., 0000-0002-5653-0401; G.Y., 0000-0003-3049-4200; Z.R.H., 0000-0002-1689-1691.

Correspondence: Steven P. Treon, Bing Center for Waldenström's Macroglobulinemia, Dana-Farber Cancer Institute, 450 Brookline Ave, Boston, MA 02215; e-mail: steven_treon@dfci.harvard.edu; and Ruben D. Carrasco, Dana-Farber Cancer Institute, 450 Brookline Ave, Boston, MA 02215; e-mail: ruben_carrasco@dfci.harvard.edu.

References

1. Varettoni M, Arcaini L, Zibellini S, et al. Prevalence and clinical significance of the MYD88 (L265P) somatic mutation in Waldenstrom's macroglobulinemia and related lymphoid neoplasms. *Blood*. 2013;121(13):2522-2528.
2. Treon SP, Xu L, Yang G, et al. MYD88 L265P somatic mutation in Waldenström's macroglobulinemia. *N Engl J Med*. 2012;367(9):826-833.
3. Jiménez C, Sebastián E, Chillón MC, et al. MYD88 L265P is a marker highly characteristic of, but not restricted to, Waldenström's macroglobulinemia. *Leukemia*. 2013;27(8):1722-1728.
4. Poulain S, Roumier C, Decambron A, et al. MYD88 L265P mutation in Waldenstrom macroglobulinemia. *Blood*. 2013;121(22):4504-4511.
5. Chapuy B, Stewart C, Dunford AJ, et al. Molecular subtypes of diffuse large B cell lymphoma are associated with distinct pathogenic mechanisms and outcomes. *Nat Med*. 2018;24(5):679-690.
6. Schmitz R, Wright GW, Huang DW, et al. Genetics and pathogenesis of diffuse large B-cell lymphoma. *N Engl J Med*. 2018;378(15):1396-1407.
7. Chapuy B, Roemer MG, Stewart C, et al. Targetable genetic features of primary testicular and primary central nervous system lymphomas. *Blood*. 2016;127(7):869-881.
8. Yu X, Li W, Deng Q, et al. *MYD88* L265P mutation in lymphoid malignancies. *Cancer Res*. 2018;78(10):2457-2462.
9. Treon SP, Tripsas CK, Meid K, et al. Ibrutinib in previously treated Waldenström's macroglobulinemia. *N Engl J Med*. 2015;372(15):1430-1440.
10. Wilson WH, Young RM, Schmitz R, et al. Targeting B cell receptor signaling with ibrutinib in diffuse large B cell lymphoma. *Nat Med*. 2015;21(8):922-926.
11. Yang G, Zhou Y, Liu X, et al. A mutation in MYD88 (L265P) supports the survival of lymphoplasmacytic cells by activation of Bruton tyrosine kinase in Waldenström macroglobulinemia. *Blood*. 2013;122(7):1222-1232.
12. Ngo VN, Young RM, Schmitz R, et al. Oncogenically active MYD88 mutations in human lymphoma. *Nature*. 2011;470(7332):115-119.
13. Avbelj M, Wolz OO, Fekonja O, et al. Activation of lymphoma-associated MyD88 mutations via allostery-induced TIR-domain oligomerization. *Blood*. 2014;124(26):3896-3904.
14. Phelan JD, Young RM, Webster DE, et al. A multiprotein supercomplex controlling oncogenic signalling in lymphoma. *Nature*. 2018;560(7718):387-391.
15. Knittel G, Liedgens P, Korovkina D, et al; German International Cancer Genome Consortium Molecular Mechanisms in Malignant Lymphoma by Sequencing Project Consortium. B-cell-specific conditional expression of Myd88p.L252P leads to the development of diffuse large B-cell lymphoma in mice. *Blood*. 2016;127(22):2732-2741.

16. Perkins DJ, Vogel SN. Inflammation: Species-specific TLR signalling -- insight into human disease. *Nat Rev Rheumatol*. 2016;12(4):198-200.

17. Morse HC III, Anver MR, Fredrickson TN, et al; Hematopathology subcommittee of the Mouse Models of Human Cancers Consortium. Bethesda proposals for classification of lymphoid neoplasms in mice. *Blood*. 2002;100(1):246-258.

18. Castillo JJ, Gustine J, Meid K, Dubeau T, Hunter ZR, Treon SP. Histological transformation to diffuse large B-cell lymphoma in patients with Waldenström macroglobulinemia. *Am J Hematol*. 2016;91(10):1032-1035.

19. Durot E, Tomowiak C, Michallet AS, et al. Transformed Waldenström macroglobulinaemia: clinical presentation and outcome. A multi-institutional retrospective study of 77 cases from the French Innovative Leukemia Organization (FILO). *Br J Haematol*. 2017;179(3):439-448.

20. Beard C, Hochedlinger K, Plath K, Wutz A, Jaenisch R. Efficient method to generate single-copy transgenic mice by site-specific integration in embryonic stem cells. *Genesis*. 2006;44(1):23-28.

21. Akbay EA, Koyama S, Liu Y, et al. Interleukin-17A promotes lung tumor progression through neutrophil attraction to tumor sites and mediating resistance to PD-1 blockade. *J Thorac Oncol*. 2017;12(8):1268-1279.

22. Robbiani DF, Bothmer A, Callen E, et al. AID is required for the chromosomal breaks in c-myc that lead to c-myc/IgH translocations. *Cell*. 2008;135(6):1028-1038.

23. Zhang J, Dominguez-Sola D, Hussein S, et al. Disruption of KMT2D perturbs germinal center B cell development and promotes lymphomagenesis. *Nat Med*. 2015;21(10):1190-1198.

24. Carrasco DR, Fenton T, Sukhdeo K, et al. The PTEN and INK4A/ARF tumor suppressors maintain myelolymphoid homeostasis and cooperate to constrain histiocytic sarcoma development in humans. *Cancer Cell*. 2006;9(5):379-390.

25. Swerdlow SH, Campo E, Harris NL, et al. WHO Classification of Tumours of Haematopoietic and Lymphoid Tissues. Vol 2. Revised 4th ed. Lyon, France: IARC Press; 2008

26. Alizadeh AA, Eisen MB, Davis RE, et al. Distinct types of diffuse large B-cell lymphoma identified by gene expression profiling. *Nature*. 2000;403(6769):503-511.

27. Pradère JP, Hernandez C, Koppe C, Friedman RA, Luedde T, Schwabe RF. Negative regulation of NF-κB p65 activity by serine 536 phosphorylation. *Sci Signal*. 2016;9(442):ra85.

28. Tanaka T, Narazaki M, Kishimoto T. IL-6 in inflammation, immunity, and disease. *Cold Spring Harb Perspect Biol*. 2014;6(10):a016295.

29. Elsawa SF, Novak AJ, Ziesmer SC, et al. Comprehensive analysis of tumor microenvironment cytokines in Waldenstrom macroglobulinemia identifies CCL5 as a novel modulator of IL-6 activity. *Blood*. 2011;118(20):5540-5549.

30. Vos JM, Tsakmaklis N, Patterson CJ, et al. CXCL13 levels are elevated in patients with Waldenström macroglobulinemia, and are predictive of major response to ibrutinib. *Haematologica*. 2017;102(11):e452-e455.

31. Abramson N. Rouleaux formation. *Blood*. 2006;107(11):4205.

32. Kristinsson SY, Koshiol J, Björkholm M, et al. Immune-related and inflammatory conditions and risk of lymphoplasmacytic lymphoma or Waldenstrom macroglobulinemia. *J Natl Cancer Inst*. 2010;102(8):557-567.

33. Atienza J, Bockorny B, Dadla A, Codreanu I, Dasanu CA. Inflammatory and immune-related conditions associated with Waldenström macroglobulinemia: a single center experience. *Leuk Lymphoma*. 2015;56(4):1179-1180.

34. Rommel PC, Bosque D, Gitlin AD, et al. Fate mapping for activation-induced cytidine deaminase (AID) marks non-lymphoid cells during mouse development. *PLoS One*. 2013;8(7):e69208.

35. Sikora KA, Bennett JR, Vyncke L, et al. Germline gain-of-function myeloid differentiation primary response gene-88 (MYD88) mutation in a child with severe arthritis. *J Allergy Clin Immunol*. 2018;141(5):1943-1947.e9.

36. Li J, Sze DM, Brown RD, et al. Clonal expansions of cytotoxic T cells exist in the blood of patients with Waldenstrom macroglobulinemia but exhibit anergic properties and are eliminated by nucleoside analogue therapy. *Blood*. 2010;115(17):3580-3588.

37. Treon SP, Gustine J, Xu L, et al. MYD88 wild-type Waldenstrom macroglobulinaemia: differential diagnosis, risk of histological transformation, and overall survival. *Br J Haematol*. 2018;180(3):374-380.

38. Jackson DA, Smith TD, Amarsaikhan N, et al. Modulation of the IL-6 receptor α underlies GLI2-mediated regulation of Ig secretion in Waldenström macroglobulinemia cells. *J Immunol*. 2015;195(6):2908-2916.

39. Burns K, Martinon F, Esslinger C, et al. MyD88, an adapter protein involved in interleukin-1 signaling. *J Biol Chem*. 1998;273(20):12203-12209.

40. Wang JQ, Jeelall YS, Beutler B, Horikawa K, Goodnow CC. Consequences of the recurrent MYD88(L265P) somatic mutation for B cell tolerance. *J Exp Med*. 2014;211(3):413-426.

41. Nagao T, Oshikawa G, Ishida S, et al. A novel MYD88 mutation, L265RPP, in Waldenström macroglobulinemia activates the NF-κB pathway to upregulate Bcl-xL expression and enhances cell survival. *Blood Cancer J*. 2015;5(5):e314.

42. Tompkins VS, Sompallae R, Rosean TR, et al. Transgenic mouse model of IgM^{+} lymphoproliferative disease mimicking Waldenström macroglobulinemia. *Blood Cancer J*. 2016;6(11):e488.

43. Castillo JJ, Olszewski AJ, Kanan S, Meid K, Hunter ZR, Treon SP. Survival outcomes of secondary cancers in patients with Waldenström macroglobulinemia: An analysis of the SEER database. *Am J Hematol*. 2015;90(8):696-701.

44. Hunter ZR, Xu L, Yang G, et al. The genomic landscape of Waldenstrom macroglobulinemia is characterized by highly recurring MYD88 and WHIM-like CXCR4 mutations, and small somatic deletions associated with B-cell lymphomagenesis. *Blood*. 2014;123(11):1637-1646.

45. Guerrera ML, Tsakmaklis N, Xu L, et al. *MYD88* mutated and wild-type Waldenström's macroglobulinemia: characterization of chromosome 6q gene losses and their mutual exclusivity with mutations in *CXCR4*. *Haematologica*. 2018;103(9):e408-e411.

46. Hunter ZR, Xu L, Yang G, et al. Transcriptome sequencing reveals a profile that corresponds to genomic variants in Waldenström macroglobulinemia. *Blood*. 2016;128(6):827-838.

47. Argyropoulos KV, Vogel R, Ziegler C, et al. Clonal B cells in Waldenström's macroglobulinemia exhibit functional features of chronic active B-cell receptor signaling. *Leukemia*. 2016;30(5):1116-1125.

48. Zhu N, Ramirez LM, Lee RL, Magnuson NS, Bishop GA, Gold MR. CD40 signaling in B cells regulates the expression of the Pim-1 kinase via the NF-kappa B pathway. *J Immunol*. 2002;168(2):744-754.

49. Jiménez C, Alonso-Álvarez S, Alcoceba M, et al. From Waldenström's macroglobulinemia to aggressive diffuse large B-cell lymphoma: a whole-exome analysis of abnormalities leading to transformation. *Blood Cancer J*. 2017;7(8):e591.

50. Nihira K, Ando Y, Yamaguchi T, Kagami Y, Miki Y, Yoshida K. Pim-1 controls NF-kappaB signalling by stabilizing RelA/p65. *Cell Death Differ*. 2010;17(4):689-698.

51. Baron BW, Anastasi J, Hyjek EM, et al. PIM1 gene cooperates with human BCL6 gene to promote the development of lymphomas. *Proc Natl Acad Sci USA*. 2012;109(15):5735-5739.

52. Peters TL, Li L, Tula-Sanchez AA, Pongtornpipat P, Schatz JH. Control of translational activation by PIM kinase in activated B-cell diffuse large B-cell lymphoma confers sensitivity to inhibition by PIM447. *Oncotarget*. 2016;7(39):63362-63373.

53. Jablonska E, Szydlowski M, Bialopiotrowicz E, et al. A novel pan-PIM kinase inhibitor, SEL24-B489, induces apoptosis and inhibits proliferation of diffuse large B-cell lymphoma cells through inhibition of protein translation and attenuation of Myc and NFkB activity [abstract]. *Blood*. 2015;126(23). Abstract 706.

54. Reddy A, Zhang J, Davis NS, et al. Genetic and functional drivers of diffuse large B cell lymphoma. *Cell*. 2017;171(2):481-494.e15.